

Simulation Studies on Advanced Microwave Diagnostics and Related Technology

Hitoshi HOJO, Atsushi MASE¹⁾ and Kazuo KAWAHATA²⁾

Plasma Research Center, University of Tsukuba, Tsukuba 305-8577, Japan

¹⁾*Art, Science and Technology Center for Cooperative Research, Kyushu University, Kasuga 816-8580, Japan*

²⁾*National Institute for Fusion Science, Toki, Gifu 509-5292, Japan*

(Received 5 December 2006 / Accepted 16 March 2007)

The full-wave Maxwell simulations on electromagnetic wave propagation based on a finite difference time domain method are performed to study the shift in cutoff density due to relativistic electron mass modification. The simulations on one-dimensional ultrashort-pulse reflectometry are also performed and the density-profile reconstruction is shown to have an underestimated density profile by the relativistic effect, and an idea of electron temperature estimation by means of reflectometry is discussed. Its related technology such as metallic wire-made discrete waveguide and beam former is also briefly discussed.

© 2007 The Japan Society of Plasma Science and Nuclear Fusion Research

Keywords: microwave diagnostic simulator, reflectometry, relativistic effect, FDTD simulation, beam former

DOI: 10.1585/pfr.2.S1022

1. Introduction

Millimeter-wave diagnostics such as reflectometry are receiving growing attention in magnetic fusion research. More detailed measurements on density profile and its fluctuations might be required in order to obtain the better understanding of plasma confinement physics. Recently, a new type of microwave reflectometry has been proposed, which is called as ultrashort-pulse reflectometry [1–10] with use of subcyclic pulses, or as imaging reflectometry [11, 12] being expected as a near-coming diagnostic. In the ultrashort-pulse reflectometry, a subcyclic pulse is an ultra-wide-band wave, and it can be considered as a set of monochromatic plane waves with various frequencies corresponding to various cutoff densities, therefore, the ultrashort-pulse reflectometry has a potential of measuring precisely the profiles of plasma density and magnetic field by only a single pulse.

In this paper, we first study numerically the relativistic effects of high-temperature electrons on electromagnetic wave propagation, which become important in burning plasma such as ITER plasmas [13–15]. We next study one-dimensional full-wave simulations on ultrashort-pulse reflectometry in high electron-temperature plasmas. In both simulations, we find the shift in the ordinary(O) or extraordinary(X) mode cutoff due to relativistic electron mass modification. We think that the present simulation on reflectometry taking into account the relativistic effect is a new attempt. The outline of our simulation model is described in the following section. The simulation scheme is based on the finite difference time domain (FDTD) method. We perform two-dimensional simulations

to study the relativistic shift of O- or X-mode cutoff density in Sec. 3 and one-dimensional simulations on O-mode ultrashort-pulse reflectometry with the density profile reconstruction in Sec. 4. The related technology on metallic wire-made discrete waveguide and beam former is discussed briefly in Sec. 5.

2. Simulation Model

In this section, we describe the simulation modeling developed in the previous works [5–10]. The basic equations to be solved are Maxwell's equation for the electromagnetic wave fields, \mathbf{E} and \mathbf{B} , and the equation of motion for the induced current density \mathbf{J} as follows:

$$\frac{\partial}{\partial t}\mathbf{B} = -\nabla \times \mathbf{E}, \quad (1)$$

$$\frac{\partial}{\partial t}\mathbf{E} = c^2\nabla \times \mathbf{B} - \frac{1}{\varepsilon_0}\mathbf{J}, \quad (2)$$

$$\frac{\partial}{\partial t}\mathbf{J} = \varepsilon_0\omega_{pe}^2\mathbf{E} - \frac{e}{m_e}\mathbf{J} \times \mathbf{B}_0, \quad (3)$$

where c is the speed of light, $\omega_{pe} (= (e^2n/m_e\varepsilon_0)^{1/2})$ the electron plasma frequency, $-e$ the charge of the electron, m_e the electron mass, n the plasma density, ε_0 the permittivity of vacuum, and \mathbf{B}_0 is the external magnetic field being dependent of plasma confinement device. In the derivation of eq. (3), we assumed that the current density \mathbf{J} is approximated as $\mathbf{J} = -en\mathbf{V}_e$, \mathbf{V}_e being the electron flow velocity, as we consider electromagnetic waves in GHz range. The above coupled equations can describe both of the ordinary (O) and extraordinary (X) modes in a plasma. When $\mathbf{B} = B_0\mathbf{e}_z$, \mathbf{e}_z being the unit vector in the z -direction,

author's e-mail: hojo@prc.tsukuba.ac.jp

the wave component E_z denotes the O mode with the dispersion relation:

$$\omega^2 = \omega_{pe}^2 + c^2 k^2, \quad (4)$$

where k is the perpendicular wavenumber. On the other hand, E_x and E_y correspond to the X mode with the dispersion relation:

$$\left(\frac{kc}{\omega}\right)^2 = 1 - \frac{\omega_{pe}^2}{\omega^2} \frac{\omega^2 - \omega_{pe}^2}{\omega^2 - \omega_{pe}^2 - \omega_{ce}^2}, \quad (5)$$

where ω_{ce} ($= eB_0/m_e c$) is the electron cyclotron frequency. The cross polarization scattering between the O and X modes due to the magnetic shear is generated from the $\mathbf{J} \times \mathbf{B}$ term in eq. (3). In the simulations, the previous equations are solved by the FDTD method.

3. Relativistic Shift of X-Mode Cutoff

In this section, we consider the relativistic effect of high electron temperature on wave propagation. The most important effect is the change of cutoff density due to the relativistic electron mass modification [13–15]. Here, the electron mass m_e is modified to $m_e(1 + 5/\mu)^{1/2}$, where $\mu = m_e c^2/T_e$, T_e being the electron temperature. In this case, the change of the cutoff density is given as follows [14]:

$$\frac{\Delta n}{n_c} = \begin{cases} \sqrt{1 + 5/\mu} - 1, & \text{(O - mode cutoff)} \\ \frac{\sqrt{1 + 5/\mu} - 1}{1 - \omega_{ce}/\omega}, & \text{(upper X-mode cutoff)} \end{cases} \quad (6)$$

where $\Delta n = n_c(\text{relativistic}) - n_c(\text{non-relativistic})$. The shift of the cutoff density due to relativistic effects is more significant for X modes.

We perform two-dimensional (x, z) FDTD simulations on X-mode propagation in a plasma with the modified electron mass, where a uniform magnetic field $\mathbf{B}_0 = B_0 \mathbf{e}_z$, $B_0 = 2$ T and a uniform electron temperature T_e are assumed, for simplicity. The density profile is given by

$$n(x) = n_0 \exp[-(\bar{x}/L_n)^2], \quad \bar{x} = x - 180, \quad (7)$$

where $n_0 = 4 \times 10^{13} \text{ cm}^{-3}$ and $L_n = 75$ mm. A X-mode beam with $\omega/2\pi = 70$ GHz is excited at $x = 0$ boundary and launched into a plasma. The incident beam has a Gaussian distribution along the z -axis. Figures 1 and 2 show the simulation results of the wave field $E_z(x)$ and Poynting vector component $S_x(x)$ at the beam center ($z = 0$). Theoretically estimated cutoff positions are $x_c = 98.2$ mm for $T_e = 0.1$ keV and $x_c = 112.5$ mm for $T_e = 20$ keV, and from Figs.1 and 2 we can see that the numerical results coincide well with the theoretical estimation.

4. Ultrashort-Pulse Reflectometry with O-Mode

In this section, we perform one-dimensional (x) FDTD simulations on O-mode ultrashort-pulse reflectometry in a plasma with the modified electron mass, where a

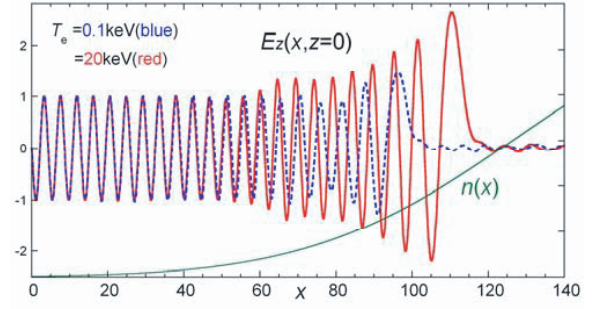


Fig. 1 Snapshots of $E_z(x)$ with $T_e = 20$ keV (solid line) and 0.1 keV (dashed line) at the beam center $z = 0$.

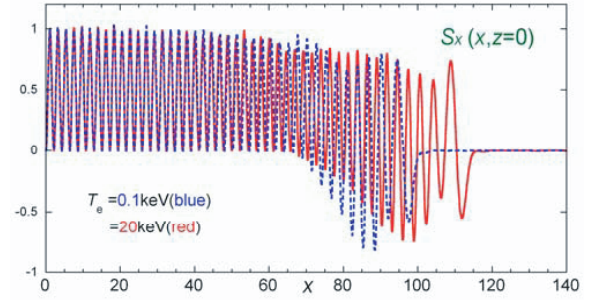


Fig. 2 Snapshots of $S_x(x)$ with $T_e = 20$ keV (solid line) and 0.1 keV (dashed line) at the beam center $z = 0$.

uniform magnetic field $\mathbf{B}_0 = B_0 \mathbf{e}_z$, $B_0 = 1$ T is assumed, and the density and electron temperature profiles are given by

$$n(x) = n_0 \exp[-(\bar{x}/L_n)^2], \quad \bar{x} = x - 1000, \quad (8)$$

$$T_e(x) = T_{e0} \exp[-(\bar{x}/L_T)^2], \quad (9)$$

where $n_0 = 2 \times 10^{13} \text{ cm}^{-3}$ and $L_n = 200$ mm, $L_T = 300$ mm and $T_{e0} = 20$, or, 100 keV. In this case, a Gaussian O-mode pulse (E_z) of the pulse width 16.7 ps (in FWHM) is excited at $x = 0$ boundary and launched into a plasma. Figure 3 shows the temporal behavior of the wave electric field E_z at $x = 200$ mm. The earlier signal at $\omega_0 t \approx 200$ shows the incident pulse and the later signal denotes the waves reflected from at the cutoff. From these reflected wave signals, we obtain the time delay $\tau(\omega)$, and we can reconstruct the density profile $n(x)$ by using the Abel inversion equation for the cutoff position x_r :

$$x_r(\omega_{pe}) = \int_0^{\omega_{pe}} d\omega \frac{c\tau(\omega)}{\pi \sqrt{\omega_{pe}^2 - \omega^2}}. \quad (10)$$

Figure 4 shows the reconstructed density profile at $x = 200$ mm (open circles) for $T_{e0} = 20$ keV (a) and 100 keV (b). The solid line shows the modeled profile $n(x)$ the dashed line denotes the density profile $n^*(x)$ with the

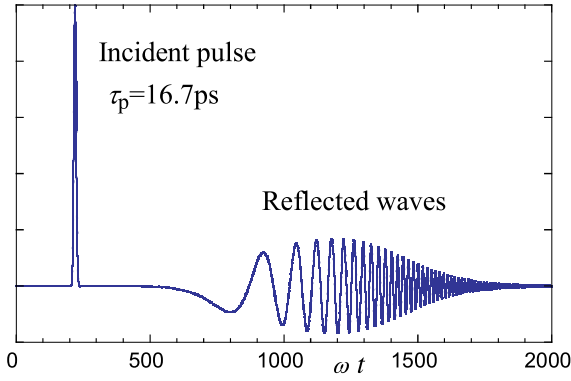


Fig. 3 The temporal evolution of $E_z(t)$ at $x = 200$ mm.

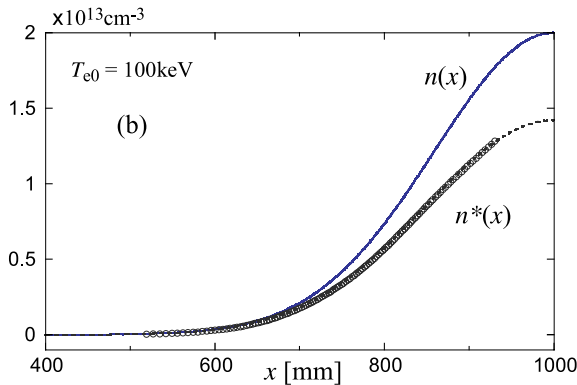
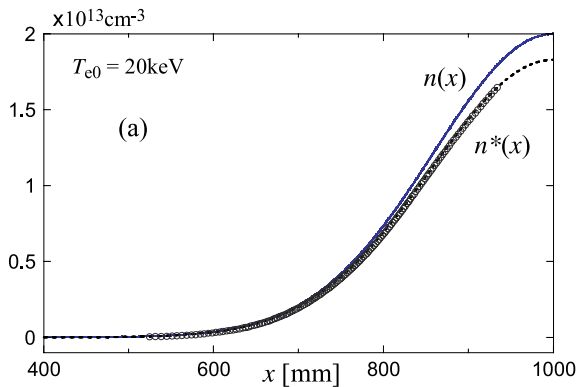


Fig. 4 The reconstructed density profile at $x = 200$ mm (open circles) for $T_{e0} = 20$ keV (a) and 100 keV (b). The solid line shows the modeled profile $n(x)$ the dashed line denotes the density profile $n^*(x)$.

relativistic mass modification given by

$$n^*(x) = \frac{n(x)}{\sqrt{1 + \frac{5T_e(x)}{m_e c^2}}} \quad (11)$$

We see that the shift in cutoff density due to the relativistic mass modification becomes larger for the higher electron temperature. The relativistic shift in cutoff density is about 17 mm at $x \approx 900$ mm for $T_{e0} = 20$ keV.

We next discuss a possibility of electron temperature profile estimation from reflectometry. When the density profile $n(x)$ is known by means of the other measurements,

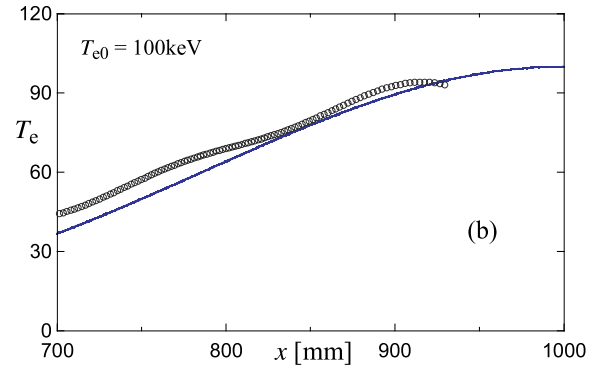
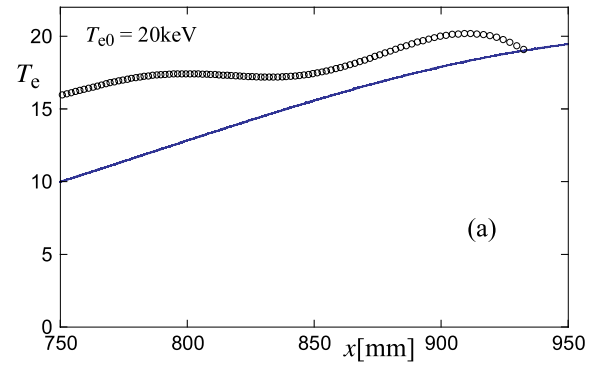


Fig. 5 The reconstructed electron temperature profile (open circles) for $T_{e0} = 20$ keV (a) and 100 keV (b). The solid line shows the modeled profile.

measuring the density profile $n^*(x)$ from reflectometry, we could estimate the electron temperature profile $T_e(x)$ from eq. (11) as

$$T_e(x) = \frac{m_e c^2}{5} \left[\left(\frac{n}{n^*} \right)^2 - 1 \right]. \quad (12)$$

Figure 5 shows the reconstructed electron temperature profiles (open circles) for $T_{e0} = 20$ keV (a) and 100 keV (b), where the reconstructed density profile data shown by open circles in Fig. 4 are used for $n^*(x)$ in eq. (12). The solid line shows the modeled profile. The reconstruction is not good for $T_{e0} = 20$ keV, however, it could provide us a rough estimation of the temperature in ITER-like plasmas. We see that the accuracy for this electron temperature estimation becomes better for the higher temperature, as the reconstruction for $T_{e0} = 100$ keV as shown in Fig. 5(b) is not bad. As the difference between $n(x)$ and $n^*(x)$ is much larger for X modes, if we use X-mode reflectometry to find $n^*(x)$, we might make an electron temperature estimation more precisely.

5. Related Technology

We here briefly discuss the technology related to the present microwave diagnostics. We have recently devised the concept of metallic wire-made discrete waveguide and beam former [16]. These devices made by metallic wires can be very flexibly assembled and applicable to electro-

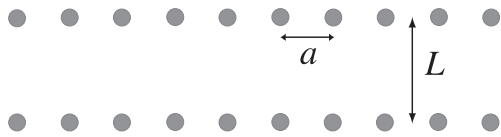


Fig. 6 2-d model of metallic wire-made discrete waveguide.

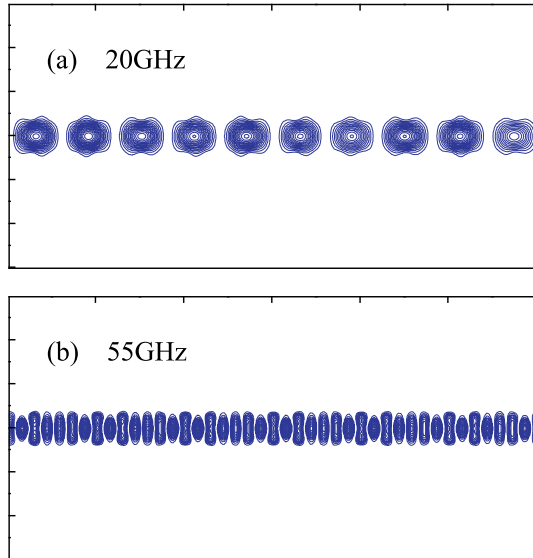


Fig. 7 Electric field distribution in metallic wire-made discrete waveguide for $\omega/2\pi = 20$ GHz (a) and 55 GHz.

magnetic waves of very wide range from microwave to optical waves.

In Figure 6, we show a two-dimensional model of metallic wire-made discrete waveguide, which is characterized by a , L and R , R being the radius of wire rod. We here demonstrate that electromagnetic wave are confined by this metallic wire-made discrete waveguide, and prop-

agate in it. Figure 7 shows the magnitude of wave electric fields of 20 GHz (a) and 55 GHz (b) propagating in a metallic wire-made discrete waveguide, where $R = 1$ mm, $a = 5$ mm and $L = 10$ mm are assumed in two-dimensional FDTD simulations. This waveguide can be applicable to frequency filters, as it has forbidden band gaps such as photonic crystals. We mention that metallic wire-made discrete beam former is also possible. The similar analysis on discrete beam former has been reported in Ref. 16.

Acknowledgments

This work was partly supported by a Grant-in-Aid for Scientific Research, the Ministry of Education, Science, Sports and Culture (“Advanced Diagnostics for Burning Plasma” No. 16082205), and also was partly performed as a collaborating program at National Institute for Fusion Science.

- [1] C.W. Domier *et al.*, Rev. Sci. Instrum. **66**, 399 (1995).
- [2] S. Kubota *et al.*, Jpn. J. Appl. Phys. **37**, L300 (1998).
- [3] S. Kubota *et al.*, Jpn. J. Appl. Phys. **38**, L202 (1999).
- [4] B.I. Cohen *et al.*, Plasma Phys. Control. Fusion **37**, 329 (1995).
- [5] H. Hojo *et al.*, Fusion Eng. Des. **34-35**, 447 (1997).
- [6] H. Hojo *et al.*, Rev. Sci. Instrum. **70**, 983 (1999).
- [7] H. Hojo *et al.*, J. Plasma Fusion Res. **78**, 387 (2002).
- [8] H. Hojo *et al.*, J. Plasma Fusion Res. **80**, 175 (2004).
- [9] H. Hojo *et al.*, Rev. Sci. Instrum. **75**, 3813 (2004).
- [10] A. Fukuchi *et al.*, J. Plasma Fusion Res. SERIES **6**, 745 (2004).
- [11] M. Ignatenko *et al.*, Rev. Sci. Instrum. **75**, 3810 (2004).
- [12] M. Ignatenko *et al.*, Nuclear Fusion **46**, S760 (2006).
- [13] I. Fidone *et al.*, Nuclear Fusion **26**, 1537 (1986).
- [14] E. Mazzucato, Phys. Fluids B **4**, 3460 (1992).
- [15] H. Bindslev, Plasma Phys. Control. Fusion **35**, 1093 (1993).
- [16] H. Hojo *et al.*, Plasma and Fusion Research **1**, 021 (2006).